Journal of Power Sources 189 (2009) 1256–1263

Contents lists available at ScienceDirect

Journal of Power Sources

journal homepage: www.elsevier.com/locate/jpowsour

A simple method to prepare uniform-size nanoparticle TiO_2 electrodes for dye-sensitized solar cells

Yongzhe Zhang, Lihui Wu, Erqing Xie*, Huigao Duan, Weihua Han, Jianguo Zhao

School of Physical Science and Technology, Lanzhou University, Tianshui Road, Lanzhou 730000, PR China

ARTICLE INFO

Article history:
Received 20 September 2008
Received in revised form 1 January 2009
Accepted 13 January 2009
Available online 20 January 2009

Keywords:
Electrostatic spray coating
Monoethanolamine
TiO_2 nanoparticles
Dye-sensitized solar cells
Recombination
Surface states

ABSTRACT

Nanoparticle TiO_2 electrodes are fabricated using an improved electrostatic spray coating (ESC) method which is more simple, low cost and well reproducible comparing with the conventional method of preparing electrode for dye-sensitized solar cells (DSSC) by introducing monoethanolamine (MEA) into precursor solution. It is surprised to find that high transparency of films and good adhesion between film and substrate achieve and that particles size can be easily controlled by adjusting the proportion of MEA. The relationship between particles size and proportion of MEA added is presented in our work. After samples with various particle sizes are applied in DSSC, an increase of open-circuit voltage (V_{oc}) from 620 mV to 765 mV is observed with the increase of particle size from 8 nm to 48 nm. Associated with photoluminescence results, we ascribe the change of V_{oc} to the different dominative states of films: surface defects and oxygen vacancies in 8 nm films, oxygen vacancy defects in 25 nm films and higher crystal quality with little of both defects in 48 nm films. In addition, different thickness films with optimized proportion of MEA is applied in DSSC, an overall light to electricity conversion efficiency (η) of 2.91% is obtained with a thickness of 2.0 μm.

1. Introduction

Recently, dye-sensitized solar cells (DSSC) have attracted widespread academic and industrial interest due to their advantages in solar energy conversion. For example, DSSC are low cost, easily fabricated, environmentally benign and have relatively high energy conversion efficiency [1–3]. In DSSC, anode films are commonly composed of high-surface-area nanostructured semiconductors to achieve sufficient dye loaded and high solar-power efficiencies. Many of studies on the preparation of nanostructured semiconductors electrodes have been reported [4–9]. However, most of the synthetic methods were high cost or involved multiple steps, such as, the fabrication and removal of templates, preparation of catalyst, and additional postsynthesis treatments. These steps would seriously affect the performance of photoanode in DSSC due to the contaminant or damage to the electrode. A most usual method is the screen-printing technology. However, it would take totally 3 days to finish the preparation of TiO_2 nanoparticles firstly, following the synthesis of TiO_2 paste and then the preparation of electrode [10]. Although using a commercially available TiO_2 powder (P25, Degussa) might be less complicated, the multi-step and poorly reproducible resulted in long-term experiments are also economically unsuitable for industrial production and has to be reduced. In addition, the film crack and poor adhesion between TiO_2 film and substrate are two serious problems for the screen-printing technology. Thus, it is crucial to find a low cost, well reproducible and simple method to prepare semiconductor electrode. Otherwise, the large-area preparation technique of photoanode is imperative for the industrial manufacture of DSSC.

On the other hand, although DSSC has been widely studied in the past two decades, some basic concepts are still controversial such as the open-circuit voltage (V_{oc}), especially the influencing factors of V_{oc}. Traditional theory explains V_{oc} as the difference between the redox level (E_{redox}) in electrolyte and the Fermi level (E_F) of photoanode in electron energies [1,11,12]:

$$V_{oc} = \frac{1}{q}(E_F - E_{redox})$$

A value of 0.7 eV for the V_{oc} is obtained according to this theory. However, various values are always observed in experiments, which reveal the disadvantage of traditional theory. It is well known that the semiconductor electrode plays an important role in the operation of DSSC and the various values of V_{oc} might arise form the different physical or chemical property of the electrode. Hence more experiments should be performed to investigate the relationship between V_{oc} and electrode property.

* Corresponding author. Tel.: +86 931 8912703; fax: +86 931 8913554.
E-mail addresses: zhangyzh04@126.com, zhangyzh04@gmail.com (Y. Zhang), xieeq@lzu.edu.cn (E. Xie).

0378-7753/$ – see front matter © 2009 Elsevier B.V. All rights reserved.
doi:10.1016/j.jpowsour.2009.01.023

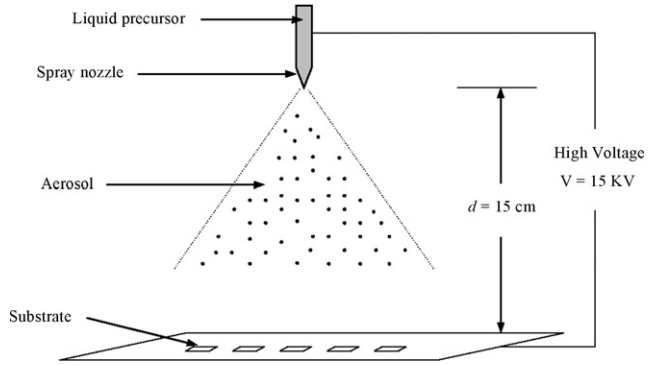

Fig. 1. Schematic drawing of the electrostatic spray coating system.

As a deposition technique, electrostatic spray coating (ESC) offers the benefits of depositing on large surfaces, coating parts with complex geometries, high deposition rate, and of being easily scaled up. In addition, ESC is a nature technique and has been widely used in industry [13] and its applications in depositing ceramic powders [14] and polymeric powders [15] have been explored. Therefore, ESC is very promising in the preparation of photoanode for the industrial manufacture of DSSC.

In our work, nanoparticle TiO_2 electrodes were fabricated by an improved ESC method and monoethanolamine (MEA) was introduced to control the particle size for the first time. A rough controlling mechanism was presented and the relationship between particles size and the proportion of MEA was given in this work. In addition, the change of V_{oc} dependence of the size of particles was studied in detail associated with photoluminescence results. With the optimized proportion of MEA, different thickness of films were prepared and applied in DSSC and their performances were also presented.

2. Experiment

The precursor solution was prepared by dissolving 0.15 g polyvinylpyrrolidone (PVP, Sigma–Aldrich, $M_w \approx 1{,}300{,}000$) in a mixed solvent formed by 2 ml ethanol and 0.5 ml *N*,*N*-dimethylformamide (DMF) beforehand. Another solution was obtained by adding 0.5 g tetrabutyl titanate (≥98%) into the mixture of 1 ml acetic acid and 1 ml ethanol. The two solutions were mixed together and MEA was added. The mixture was stirred for 1 h, and then loaded into a 2 ml glass syringe equipped with an 8-mm-gauge stainless steel needle. As shown in Fig. 1, the needle was connected to a high voltage of 15 kV. A big piece of grounded zinc flake was placed 15 cm away below the tip of the needle. FTO substrates (4 mm in thickness, 75% transmittance in visible region, 35 Ω/□) were placed on the zinc flake to collect the sprayed nanoparticles. The film thickness and growth rate were controlled by changing the spray time and adjusting the weight added on the syringe, respectively. Finally, all samples were annealled at 450 °C in air for 30 min to remove the organic compounds. By adjusting the MEA proportion (0.00, 1.58, 1.86, 2.43, 3.43 and 8.49 wt% versus the total weight of precursor solution), samples M_0, M_1, M_2, M_3, M_4 and M_5 were prepared (with nearly the same thickness about 1 μm). Moreover, different thickness TiO_2 films signed as T_1, T_2, T_3 and T_4 were also fabricated with 1.58 wt% MEA.

To prepare the DSSC, the samples were soaked in 3×10^{-4} M of ruthenium(II) dye (known as N719) in a *t*-butanol/acetonitrile (1:1, v/v) solution for 24 h at room temperature, and they were then rinsed with ethanol to remove excess dye on the surface and air-dried at room ambient. The cells whose active area was about 1 cm^2 was fabricated by using the dye-adsorbed TiO_2 photoanode and a thermally platinized counter electrode (7 mM H_2PtCl_6 in isopropanol, heated at 400 °C on FTO for 15 min) filled with acetonitrile solution containing 0.05 M of I_2, 0.1 M of LiI and 0.5 M of 4-*tert*-butylpyridine.

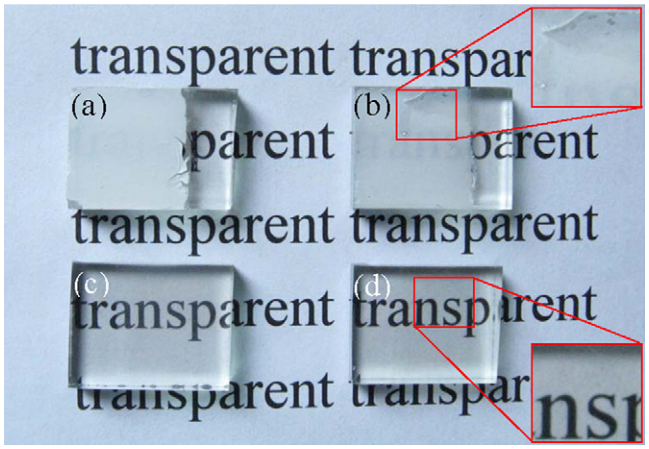

Fig. 2. Photographs of the samples without and with MEA added.

The structural properties of films were studied by X-ray diffraction (XRD) (Philips X'pert Pro MPD (Cu Kα ray)). Raman scattering spectra was performed on a Jobin-Yvon LabRam HR80 spectrometer (with a 532 nm line of Torus 50 mW diode-pumped solid-state laser) under the backscattering geometry. The morphology and thickness of samples were investigated by field emission scanning electron microscopy (FESEM) (Hitachi, S-4800). Room-temperature photoluminescence (PL) spectra (excitation source: He–Cd laser) were performed to study the crystal properties. Photocurrent–voltage curves were measured under simulated solar light (AM 1.5, 100 mW/cm^2).

3. Results and discussion

Fig. 2 shows the visual images of the samples without (a) and with MEA (c) and the corresponding annealed samples (b) and (d). For the samples without MEA, the adhesion between TiO_2 film and substrate is very bad which could be seen from the edge of the TiO_2 film in Fig. 2(a) and the magnification picture in Fig. 2(b). For the thinner samples without MEA, cracks appear after annealing (shown in Fig. S1) and the problem of cracks becomes serious for the thicker samples. It was observed that almost all the films peel off FTO after annealing for the thicker ones (shown in Fig. S2). The similar phenomena have also been reported in previous works [16–20]. It is surprising that the phenomenon of bad adhesion is greatly improved after adding MEA shown in Fig. 2(c) and (d). Moreover, it is obvious that the transparency of samples is also greatly enhanced by the introduction of MEA, which could much enhance the absorption of photons by dye.

Fig. 3 shows the SEM images demonstrating the morphologies and thickness of the TiO_2 films. For the samples without MEA, as shown in Fig. 3(a), TiO_2 nanofibers are synthesized and they accumulate together loosely. After introducing MEA, uniform-size TiO_2 nanoparticles are obtained and the particle size become larger with the increase of the MEA proportion added into the precursor solution. For the sample M_1, the size is uniform about 8 nm. When MEA proportion increases up to 3.43 wt% (sample M_4), as shown in Fig. 3(e), the TiO_2 film is composed of particles varied in size. In Fig. 3(f), the size increases to about 40 nm with 8.49 wt% MEA (sample M_5) added. The increase of particle size may be due to the following reason: when MEA was introduced into precursor solution, it could disperse in the mixture uniformly by strong stir. In the spray progress, accompanied with the volatilization of solvent,

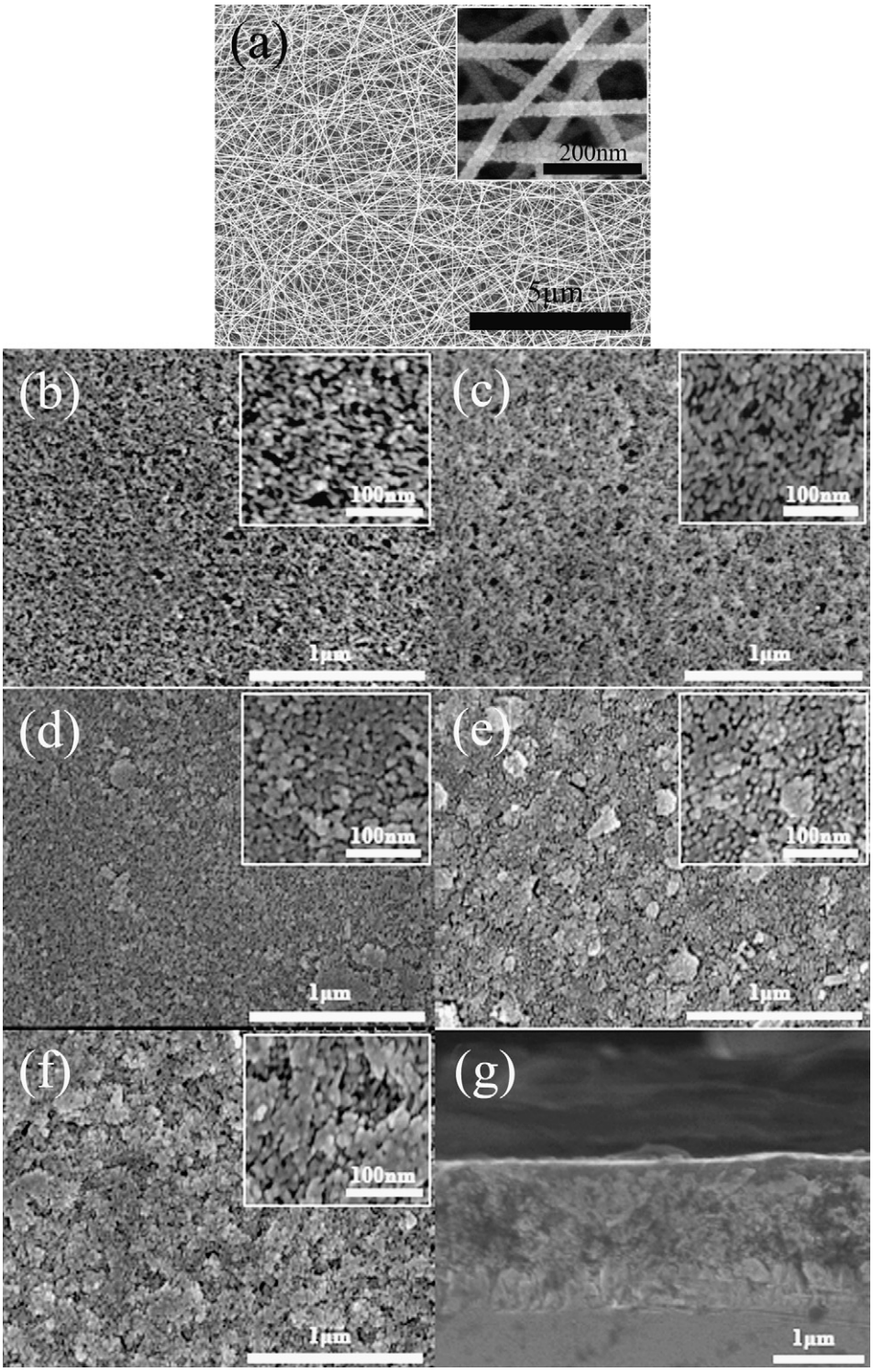

Fig. 3. FESEM images of samples without MEA (a) and with different proportion of MEA added (b) M_1, (c) M_2, (d) M_3, (e) M_4, (f) M_5 and (g) the cross sectional view of the sample M_1.

the MEA aggregated to form separate dips which contain numbers of titanate molecules due to its mucous property. Then the uniform nanoparticles were obtained after annealing. The more MEA added, the big dip consisted of more titanate molecules formed and then larger particles were achieved. However, when abundant MEA existed in spray mixture, the larger dip would separate into small ones varied in volume due to the extensive presence of charge under high voltage. Thus varied size of particles appeared such as the sample M_5. Therefore, the particle size could be easily controlled by the introduction of MEA. From the cross-section of the sample shown in Fig. 3(g), a good adhesion of spray film to the FTO appears and all the films thickness are about 1.0 μm (about 0.5, 1.5 and 2.0 μm for samples T_1, T_3 and T_4, the others not shown here).

Fig. 4(a)–(d) shows the XRD patterns, Raman scattering spectra of samples with different MEA proportion and thickness and the relationship between particle size and the proportion of MEA. The XRD patterns of FTO, M_1, M_2, M_3, M_4, M_5 are shown in Fig. 4(a), in which two typical peaks (1 0 1) and (2 0 0) of anatase TiO_2 are

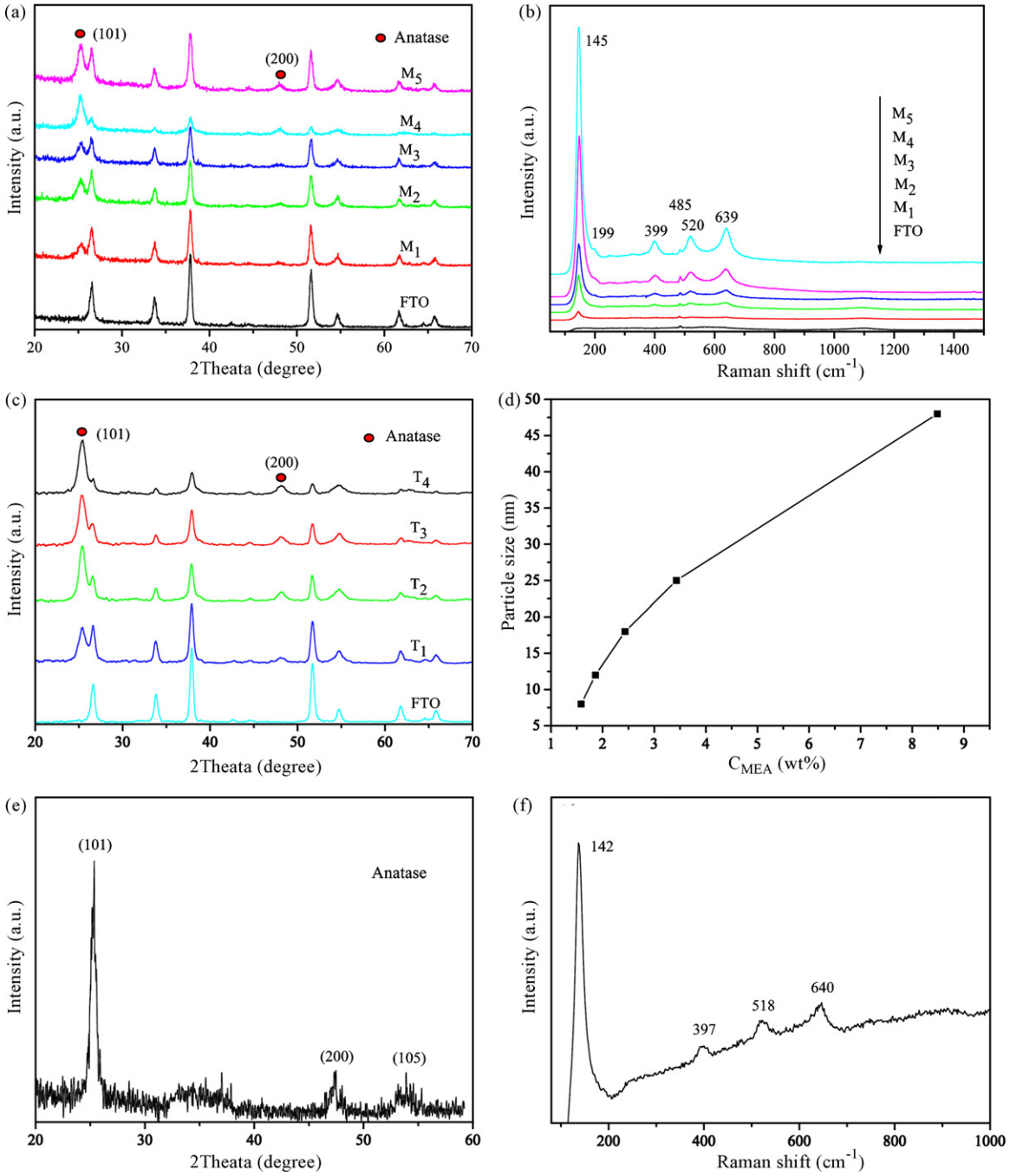

Fig. 4. XRD patterns (a) and Raman scattering spectra (b) of samples M_1, M_2, M_3, M_4 and M_5 (c) XRD patterns of samples T_1, T_2, T_3 and T_4. (d) Relationship between particle size and the proportion of MEA added. XRD patterns (e) and Raman scattering spectra (f) of sample without MEA.

observed [21–23]. It can be obviously seen that the full width at half maximum (FWHM) of (1 0 1) peak became narrow with more MEA added. The average grain size of the samples is estimated by Scherrer formula:

$$D = \frac{0.89\lambda}{B\cos\theta}$$

where D, λ, θ and B is the mean grain size, the X-ray wavelength (here is 0.154056 nm), the Bragg diffraction angle and FWHM of (1 0 1) peak, respectively. The average grain size is achieved about 8 nm, 12 nm, 18 nm, 25 nm and 48 nm for M_1, M_2, M_3, M_4, M_5, respectively, which is roughly consistent with the results of SEM.

Fig. 4(b) shows the Raman scattering spectra of the samples with different proportion of MEA added. The Raman scattering spectra are performed to investigate the vibrational properties of the TiO_2 nanostructures. Anatase-structured TiO_2 belongs to the D_{4h} space group [24,25]. In Fig. 4(a), six Raman modes are observed at 145, 199, 399, 485, 520 and 639 cm^{-1}. Among them, the peak at 485 cm^{-1} arises from FTO substrate and peaks at 145, 199, 399, 520 and 639 cm^{-1} should be assigned to the E_g, B_{1g}, A_{1g}, B_{2g} and E_g mode, respectively [26,27]. As shown in Fig. 4(b), all samples maintain the only anatase phase.

Fig. 4(c) shows the XRD pattern of samples with various thicknesses. All the samples maintain typical anatase TiO_2 structure. Estimating the average grain size by Scherrer formula, a value about 8 nm is obtained for all samples, indicating that there is no relation between film thickness and particle size. Otherwise, the diffraction peaks belonged to FTO become lower which reveals an increase in

film thickness. The relation between particle size and MEA proportion is showed in Fig. 4(d). The particle size could be controlled by MEA proportion, which is technical significant for DSSC industrial production. Moreover, the samples without MEA also maintain typical anatase TiO_2 structure which could be confirmed from the XRD and Raman scattering results shown in Fig. 4(e) and (f).

It is known that all type defects could influence the charge transfer in DSSC and play different roles in the DSSC operation. In order to investigate the crystal quality of electrodes, room-temperature PL spectra from samples M_1, M_4, M_5 are measured as shown in Fig. 5. PL measurement is a powerful technique to investigate energy levels in the band-gap and the electronic structure, optical and photochemical properties of semiconductor materials, by which the information such as surface oxygen vacancies (SOVs) and defects, as well as the efficiency of charge carrier trapping, immigration and transfer could be obtained [28–32]. As shown in Fig. 5, two UV emissions located at 365 nm (3.4 eV) and 369 nm (3.36 eV) are observed clearly from all samples and emission intensities become larger with the increase of particle size. Pan et al have also observed the PL band with maximum peak at 3.40 eV and attributed it to the band-to-band recombination because it is near-band-edge luminescence [33]. It can be seen that the band including the peaks at 3.40 and 3.36 eV can be fitted into seven Gaussian peaks as shown in the inset of Fig. 5(c). Furthermore, the half-width of those peaks is the identical with each other and the energy interval between neighboring fitted peaks is all about 0.04 eV. According to the Raman spectrum above, the sum of optical phonon energy of E_g (0.0180 eV) and B_{1g} (0.0247 eV) is 0.0427 eV, almost equal to the 0.04 eV interval. Because the k location of E_V top and E_C bottom is not at the same position in k space according to the energy band structure of TiO_2 [34], some optical phonons are needed to assist the recombination in order to keep momentum conservation in the band-to-band optical transition, including optical phonon absorption and emission. Conclusively, we attribute this PL band to the band-to-band recombination with the participation of phonons represented as E_g and B_{1g} and a similar phenomenon has also been observed in previous work [35]. As the UV emission is assisted by phonons, the crystal quality of TiO_2 which is concerned with phonons will be explored by the UV emission. It is observed that the UV emission intensity become larger when the particle size increases. As the particle size decreases, the surface to volume fraction would increase immediately and numbers of defects located at surface or inner form, which both would decrease the crystal quality of films.

In the visible region, a hump is observed which could be fitted by four Gaussian peaks as shown in the inset of Fig. 5(a). They are located at about 390 nm, 416 nm, 460 nm and 545 nm, respectively. The peak at 390 nm observed from all samples might be assigned to the free exciton recombination below conductive band. With the decrease of quality crystal, the emission intensity located at 416 nm observed from all samples become larger. Here, it is reasonable to ascribe them to bulk defects. In basic TiO_2 cells, each Ti^{4+} is surrounded by an octahedron of six O^{2-} ions, structural defects can be formed by losing neutral oxygen atoms and vacancy states associated with Ti^{3+} ions are introduced. Otherwise, oxygen vacancies can easily form because of the higher surface to volume ratio of nanoparticles. Then self-trapped excitons localized on TiO_6 octahedral could be achieved when oxygen vacancies trap electrons (F, an oxygen-ion vacancy occupied by two electron and F^+, an oxygen-ion vacancy occupied by one electron centers [36]). In our opinion, the 416 nm peak is attributed to the self-trapped excitons localized on TiO_6 octahedral. Similar phenomena have also been observed in the previous work [37–40]. The 460 nm and 545 nm are only observed in the samples with small particle size. In nanocrystals, surfaces play particularly important roles since the surface-to-volume ratio becomes larger. By introducing surface states formed near the surface (e.g. ion vacancies, surface ions with

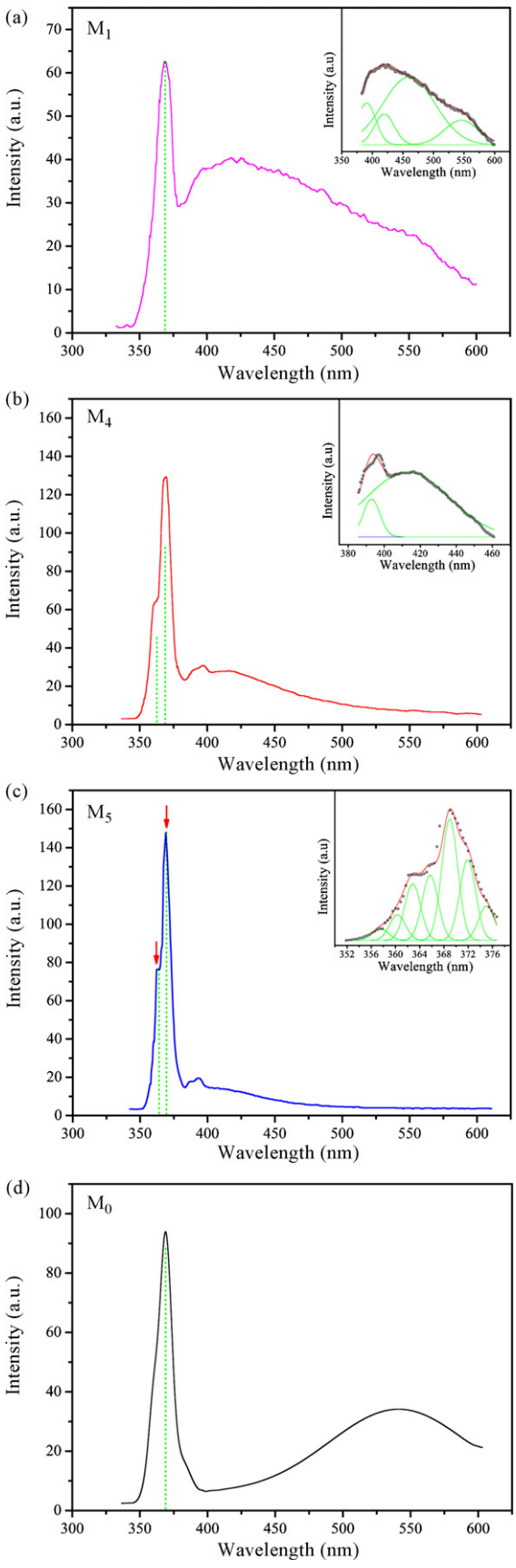

Fig. 5. Room-temperature PL spectra from samples M_1, M_4, M_5, M_0 and the inset is the corresponding Gaussian fit.

Table 1
Summary of the V_{oc}, J_{sc}, FF and η of the samples M_0, M_1, M_4 and M_5 (a) and (b) samples T_1, T_2, T_3 and T_4.

Sample	V_{oc} (mV)	J_{sc} (mA/cm^2)	FF (%)	η (%)
(a)				
M_0	648	0.41	45.6	0.12
M_1	620	3.92	61.3	1.49
M_4	699	1.80	44.1	0.56
M_5	765	1.09	59.8	0.50
(b)				
T_1	637	2.59	60.0	0.99
T_2	620	3.92	61.3	1.49
T_3	629	4.80	54.4	1.64
T_4	629	7.89	58.5	2.91

low coordination numbers, and groups coordinated on the surface of materials), localized energy levels are introduced in the middle of forbidden band gap. These mid-gap surface states are expected to become luminescence centers under an appropriate excitation [41]. Therefore, the two peaks might be assigned to the involvement of mid-gap surface states. The surface states could be formed by the surface ions with low coordinate number, e.g. Ti^{3+}, oxygen vacancies, and groups coordinated on the surface of TiO_2 such as TiOH, $TiOC_4H_9OH$, etc. The first emission band around 466 nm of TiO_2 nanocrystals could be due to the surface states formed by oxygen vacancy (F) [37], and the other band around 545 nm might be due to the surface states formed by Ti^{3+} according to [29,42] or the F^+-type color center on the surface of TiO_2 nanocrystals [37]. For the samples without MEA, as shown in Fig. 5(d), a broad emission band centered at 540 nm appears, which indicates that there are also some defects existed in the nanofibers.

Fig. 6 shows the *J–V* characteristics of the TiO_2 nanofibers and nanopaticles based dye sensitized solar cells under 100 mW/cm^2 simulated AM 1.5 G sunlight. Table 1 summarizes the measured and calculated values obtained from each *J–V* curve in Fig. 6. The FF and η for each solar cell are calculated from the following equations [43]:

$$\text{FF}\ (\%) = \left[\frac{V_{\max} \times J_{\max}}{V_{oc} \times J_{sc}}\right] \times 100$$

$$\eta\ (\%) = \left[\frac{\text{FF} \times V_{oc} \times J_{sc}}{P_{\text{source}}}\right] \times 100$$

where the $V_{\max}$, $J_{\max}$, P_{source} are the maximum voltage point, the maximum current density and the power density of incident light, respectively. In this experiment, the P_{source} is fixed at 100 mW/cm^2.

As shown in Fig. 6(a), for the nanofibers based cells, J_{sc} and η are found to be 0.41 mA/cm^2 and 0.12%, respectively. Both of them are much lower than these of the samples with MEA as shown in Table 1. This might be due to the following reasons: (1) for the nanofibers based DSSC, nanofibers accumulate together loosely and the FTO could not be fully covered by nanofibers (shown in Figs. S3 and S4). These may cause larger dark current occurred between the electrons in FTO and I_3^- in electrolyte, which could reduce J_{sc} extremely. The similar results have also been reported in previous work [44]. However, the samples with MEA show a perfect contact between TiO_2 film and FTO. Thus a higher J_{sc} achieves. (2) Compared with nanoparticls, nanofibers possess lower surface area. So less dye is loaded which caused low J_{sc} and low η.

Among the samples with MEA, sample M_1 possesses the lowest V_{oc} and the V_{oc} increases as the particle size become larger. Associated with the PL results, it is found that the three samples possess different states. One is with extrinsic (surface states) and intrinsic defects (oxygen vacancy), another is with intrinsic defects (oxygen vacancy) and the last is with few defects as high quality crystal.

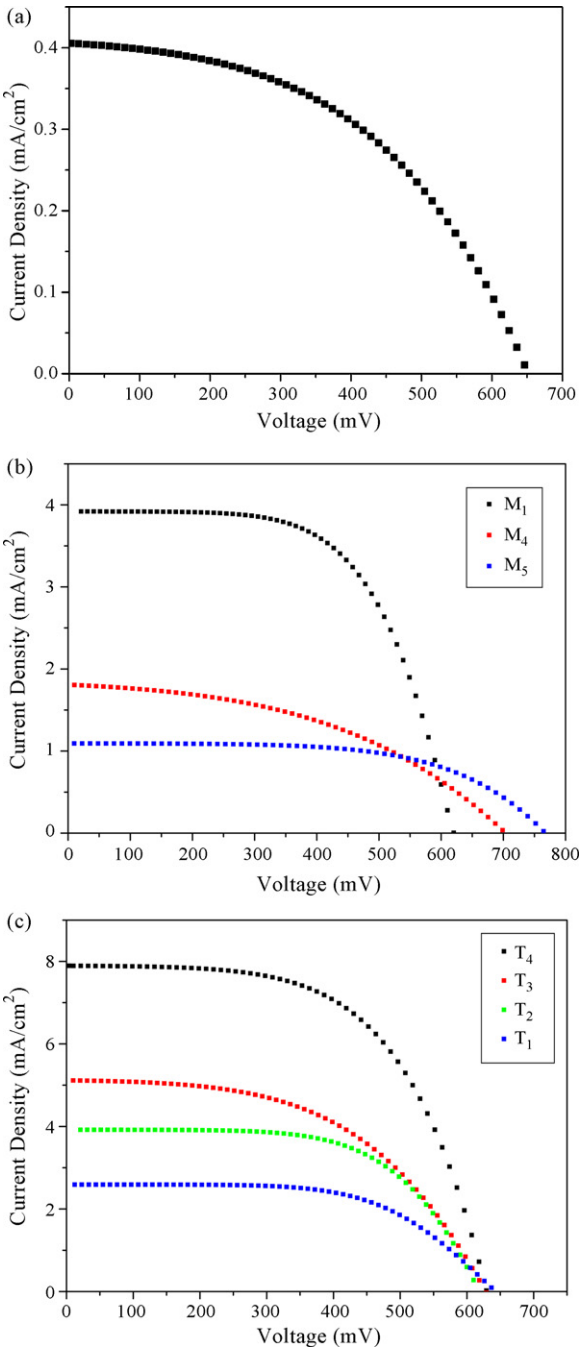

Fig. 6. Plots of the *J–V* behavior of solar cells consisting of TiO_2 films for samples M_0 (a) M_1, M_4 and M_5, and (b), T_1, T_2, T_3 and T_4 (c).

As mentioned above, as the charge carrier transport in cells operation, the quality of semiconductor films especial the defect type would influence factors of cell operation directly. Thus the change of V_{oc} could be due to three different states for nanoparticle TiO_2 as shown in Fig. 7: when sample possesses a high quality crystal, photoelectrons inject into the conduction band of TiO_2 and transport through semiconductor photoanode quickly. The quasi-Fermi level (E_{Fn}) of electrons is located at a higher energy region which would introduce a high V_{oc} as shown in Fig. 7(a). When sample possesses numbers of intrinsic defects (oxygen vacancy), part of these photoinjected electrons are trapped in oxygen vacancy. Then the dark current would increase and the E_{Fn} decreases due to the electron occupancy in these oxygen vacancies in the positive region of E_{FB}. The E_{Fn} would decrease and V_{oc} degrades synchronously as

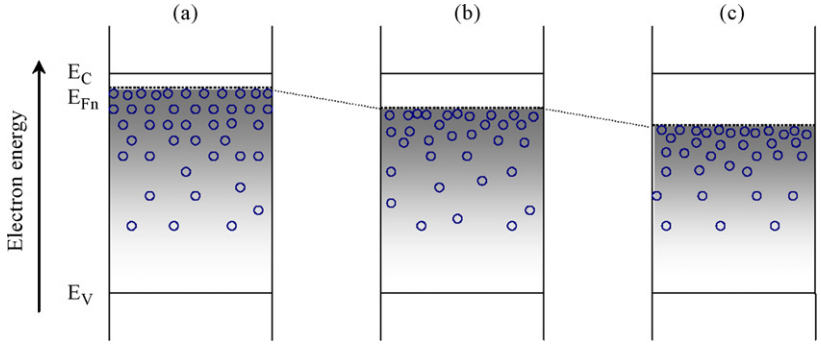

Fig. 7. Simple diagram showing the position of E_{Fn} and the distribution of the defect states in the band gap region for the (a) M_5, (b) M_4 and (c) M_1.

shown in Fig. 7(b). When sample possesses numbers of extrinsic (surface states) in addition to intrinsic defects (oxygen vacancy), the photoinjected electrons are trapped in surface states [45–47] in the concentrated and wide distribution in the positive region of E_{Fn}. The positive shift of E_{Fn} in electrode may be assumed and the further degradation of V_{oc} is observed corresponded from the existence of a large amount of trap sites in the positive potential region of E_{Fn} as shown in Fig. 7(c). While the enhancement of photocurrent is due to the increased dye adsorption from the increased surface area, despite of minor side effect such as electron loss by trapping/detrapping events and increased charge recombination. As discussed above, the variations of V_{oc} might be induced by different kinds of defects and all phenomena are consisting with previous work [48,49].

Due to the good performance in η of sample M_1, varied thickness films with 1.58 wt% MEA were prepared. As shown in Fig. 6(b) and Table 1(b), the J_{sc} and η are greatly improved when thickness increases and the V_{oc} and FF almost maintain the same value. The invariability on the V_{oc} and FF may be due to the same surface chemistry of oxide anode and the uniform particle size about 8 nm [50]. For the J_{sc}, as it is reported before, the amount of dye loaded affects the J_{sc} directly. When the thickness of the TiO_2 film increases from 0.5 to 2.0 μm, more dyes load, the J_{sc} and η are greatly enhanced.

4. Conclusions

In this work, nanoparticle TiO_2 films were fabricated using ESC method and MEA was introduced for the first time. Compared with the usual preparation method of electrode, ESC is more simple, low cost and well reproducible. The transparency of samples and the adhesion between TiO_2 film and substrate were greatly improved as the introduction of MEA into the conventional ESC. In addition, the size of TiO_2 particles could be easily controlled by adjusting the proportion of MEA. The relationship between particles size and the proportion of MEA was presented in our experiment. After samples with various particle sizes been applied in DSSC, an increase of V_{oc} from 620 mV to 765 mV was observed with the increase of particle sizes from 8 nm to 48 nm. By analyzing the PL results, we attributed the change of V_{oc} to three different states for nanoparticle TiO_2, with extrinsic (surface states) and intrinsic defects (oxygen vacancy), with intrinsic defects (oxygen vacancy), and with few defects as high quality crystal. Moreover, different thickness of samples with the optimized proportion of MEA was applied in DSSC, an overall light to electricity conversion efficiency of 2.91% was achieved with a thickness of 2.0 μm. The method of improved ESC could also be extended to prepare nanoparticles of other inorganic materials. All results could be significant to understand the micro-progress in cells and provide guide for large-area preparation of DSSC electrode in industrial manufacture.

Acknowledgments

This work is supported by the Program for New Century Excellent Talents in University (Grant No. NCET-04-0975) and the National Found for Fostering Talents of Basic Science (NFFTBS No. J0630313).

Appendix A. Supplementary data

Supplementary data associated with this article can be found, in the online version, at doi:10.1016/j.jpowsour.2009.01.023.

References

[1] B. O' Regan, M. Grätzel, Nature 353 (1991) 737–740.
[2] M. Grätzel, J. Photochem. Photobiol. C 4 (2003) 145–153.
[3] M. Grätzel, J. Photochem. Photobiol. A 164 (2004) 3–14.
[4] A.J. Cheng, Y. Tzeng, Y. Zhou, M. Park, T.H. Wu, C. Shannon, D. Wang, W. Lee, Appl. Phys. Lett. 92 (2008) 092113.
[5] S.J. Wu, H.W. Han, Q.D. Tai, J. Zhang, B.L. Chen, S. Xu, C.H. Zhou, Y. Yang, H. Hu, X.Z. Zhao, Appl. Phys. Lett. 92 (2008) 122106.
[6] T.H. Meen, C.J. Huang, Y.W. Chen, L.W. Ji, C.C. Diao, H.H. Chung, Key Eng. Mater. 368–372 (2008) 1716–1719.
[7] A.B.F. Martinson, J.W. Elam, J.T. Hupp, M.J. Pellin, Nano Lett. 7 (2007) 2183–2187.
[8] I. Kartini, D. Menzies, D. Blake, J.C.D. da Costa, P. Meredith, J.D. Riches, G.Q. Lu, Mater. Chem. 14 (2004) 2917–2921.
[9] S. Takenaka, Y. Maehara, H. Imai, M. Yoshikawa, S. Shiratori, Thin Solid Films 438–439 (2003) 346–351.
[10] S. Ito, P. Chen, P. Comte, M.K. Nazeeruddin, P. Liska, P. Pechy, M. Grätzel, Prog. Photovolt.: Res. Appl. 15 (2007) 603–612.
[11] J. van de Lagemaat, N.G. Park, A.J. Frank, J. Phys. Chem. B 104 (2000) 2044–2052.
[12] D. Cahen, G. Hodes, M. Grätzel, J. Francüois, G.I. Riess, J. Phys. Chem. B 104 (2000) 2053–2059.
[13] J.F. Hughes, Electrostatic Powder Coating, John Wiley and Sons Inc., 1984.
[14] S.N. Yedave, A.P. Malshe, W.D. Brown, W.C. Russell, Trans. NAMRI/SME XXX (2002) 486.
[15] M.K. Mazumder, D.L. Wankum, R.A. Sims, J.R. Mountain, H. Chen, P. Pettit, T. Chaser, J. Electrostat. 40–41 (1997) 369–374.
[16] H. Kokubo, B. Ding, T. Naka, H. Tsuchihira, S. Shiratori, Nanotechnology 18 (2007) 165604.
[17] I.-D. Kim, J.M. Hong, B.H. Lee, D.Y. Kim, Appl. Phys. Lett. 91 (2007) 163109.
[18] M.Y. Song, D.K. Kim, S.M. Jo, D.Y. Kim, Synth. Met. 155 (2005) 635–638.
[19] M.Y. Song, Y.R. Ahn, S.M. Jo, D.Y. Kim, Appl. Phys. Lett. 87 (2005) 113113.
[20] M.Y. Song, D.K. Kim, K.J. Ihn, S.M. Jo, D.Y. Kim, Nanotechnology 15 (2004) 1861–1865.
[21] S. Nakade, M. Matsuda, S. Kambe, Y. Saito, T. Kitamura, T. Sakata, Y. Wada, H. Mori, S. Yanagida, J. Phys. Chem. B 106 (2002) 10004–10010.
[22] K.H. Ko, Y.C. Lee, Y.J. Jung, J. Colloid Interface Sci. 283 (2005) 482–487.
[23] S. Pavasupree, Y. Suzuki, S.P. Art, S. Yoshikawa, Sci. Technol. Adv. Mater. 6 (2005) 224–229.
[24] N.G. Park, G. Schlichthoerl, J. van de Lagemaat, H.M. Cheong, A. Mascarenhas, A.J. Frank, J. Phys. Chem. B 103 (1999) 3308–3314.
[25] F.R.F. Fan, A.J. Bard, J. Phys. Chem. 94 (1990) 3761–3766.
[26] T. Ohsaka, F. Izumi, Y. Fujiki, J. Raman Spectrosc. 7 (1978) 321–325.
[27] H.J. An, S.R. Jang, R. Vittala, J. Lee, K.J. Kim, Electrochim. Acta 50 (2005) 2713–2718.
[28] Y.Z. Zhang, L.H. Wu, H. Li, J.H. Xu, L.Z. Han, B.C. Wang, Z.L. Tuo, E.Q. Xie, J. Alloys Compd. 473 (2009) 319–322.
[29] J.C. Yu, J.G. Yu, W.K. Ho, Z.T. Jiang, L.Z. Zhang, Chem. Mater. 14 (2002) 3808–3816.
[30] M. Anpo, N. Aikawa, Y. Kubokawa, M. Che, C. Louis, E. Giamello, J. Phys. Chem. 89 (1985) 5689–5694.
[31] W.F. Zhang, M.S. Zhang, Z. Yin, Q. Chen, Appl. Phys. B 70 (2000) 261–265.

[32] L.Q. Jing, X.J. Sun, W.M. Cai, Z.L. Xu, Y.G. Du, H.G. Fu, J. Phys. Chem. Solids 64 (2003) 615–623.
[33] D. Pan, N. Zhao, Q. Wang, S. Jiang, X. Ji, L. An, Adv. Mater. 17 (2005) 1991–1995.
[34] M. Grätzel, Heterogeneous Photochemical Electron Transfer, XRC Press, Inc., 1989.
[35] B.S. Liu, L.P. Wen, X.J. Zhao, Mater. Chem. Phys. 106 (2007) 350–353.
[36] D.R. Vij, N. Singh, Luminescence and Related Properties of II–IV Semiconductors, NOVA Science Publishers, Inc., Commack, New York, 1998, p. 320.
[37] Y. Lei, L.D. Zhang, G.W. Meng, G.H. Li, X.Y. Zhang, C.H. Liang, W. Chen, S.X. Wang, Appl. Phys. Lett. 78 (2001) 1125.
[38] H. Tang, H. Berger, P.E. Schmid, F. Levy, Solid State Commun. 87 (1993) 847–850.
[39] L.V. Saraf, S.I. Patil, S.B. Ogale, S.R. Sainkar, S.T. Kshirsager, Int. J. Mod. Phys. B 12 (1998) 2635–2647.
[40] J.M. Wu, H.C. Shih, W.T. Wu, Y.K. Tseng, I.C. Chen, J. Cryst. Growth 281 (2005) 384–390.
[41] A. Emeline, G.V. Kataeva, A.S. Litke, A.V. Rudakova, V.K. Ryabchuk, N. Serpone, Langmuir 14 (1998) 5011–5022.
[42] Y.C. Zhu, C.X. Ding, J. Solid State Chem. 145 (1999) 711–715.
[43] M. Grätzel, Nature 414 (2001) 338–344.
[44] K. Onozuka, B. Ding, Y. Tsuge, T. Naka, M. Yamazaki, S. Sugi, S. Ohno, M. Yoshikawa, S. Shiratori, Nanotechnology 17 (2006) 1026–1031.
[45] I.A. Shkrob, M.C. Sauer, J. Phys. Chem. B 108 (2004) 12497–12511.
[46] A.C. Fisher, L.M. Peter, K.G.U. Wijayantha, J. Phys. Chem. B 104 (2000) 949–958.
[47] A. Hagfeldt, M. Gratzel, J. Phys. Chem. 100 (1996) 8045–8048.
[48] J. Bisquert, A. Zaban, M. Greenshtein, I.M. Sero, J. Am. Chem. Soc. 126 (2004) 13550–13559.
[49] S.H. Kang, J.Y. Kim, Y.K. Kim, Y.E. Sung, J. Photochem. Photobiol. A: Chem. 186 (2007) 234–241.
[50] T.P. Chou, Q.F. Zhang, G.E. Fryxell, G.Z. Cao, Adv. Mater. 19 (2007) 2588–2592.